IEEE ComSoc IEEE Communications Society | IEEE COMPUTER SOCIETY | IEEE Signal Processing Society | VTS Connecting the Mobile World | IEEE Transactions on Machine Learning in Communications and Networking

Received 10 February 2025; revised 6 May 2025 and 14 June 2025; accepted 4 July 2025.
Date of publication 10 July 2025; date of current version 30 July 2025.

The associate editor coordinating the review of this article and approving it for publication was M. Chen.

Digital Object Identifier 10.1109/TMLCN.2025.3587205

User Handover Aware Hierarchical Federated Learning for Open RAN-Based Next-Generation Mobile Networks

AMARDIP KUMAR SINGH (Student Member, IEEE), AND KIM KHOA NGUYEN

Department of Electrical Engineering, École de Technologie Supérieure, Montreal, QC H3C 1K3, Canada

CORRESPONDING AUTHOR: A. K. SINGH (amardip-kumar.singh.1@ens.etsmtl.ca)

ABSTRACT The Open Radio Access Network (O-RAN) architecture, enhanced by its AI-enabled Radio Intelligent Controllers (RIC), offers a more flexible and intelligent solution to optimize next generation networks compared to traditional mobile network architectures. By leveraging its distributed structure, which aligns seamlessly with O-RAN's disaggregated design, Federated Learning (FL), particularly Hierarchical FL, facilitates decentralized AI model training, improving network performance, reducing resource costs, and safeguarding user privacy. However, the dynamic nature of mobile networks, particularly the frequent handovers of User Equipment (UE) between base stations, poses significant challenges for FL model training. These challenges include managing continuously changing device sets and mitigating the impact of handover delays on global model convergence. To address these challenges, we propose MHORANFed, a novel optimization algorithm tailored to minimize learning time and resource usage costs while preserving model performance within a mobility-aware hierarchical FL framework for O-RAN. Firstly, MHORANFed simplifies the upper layer of the HFL training at edge aggregate servers, which reduces the model complexity and thereby improves the learning time and the resource usage cost. Secondly, it uses jointly optimized bandwidth resource allocation and handed over local trainers' participation to mitigate the UE handover delay in each global round. Through a rigorous convergence analysis and extensive simulation results, this work demonstrates its superiority over existing state-of-the-art methods. Furthermore, our findings underscore significant improvements in FL training efficiency, paving the way for advanced applications such as autonomous driving and augmented reality in 5G and next-generation O-RAN networks.

INDEX TERMS Hierarchical federated learning, FL, open RAN, O-RAN intelligent controllers, handover, mobility, B5G.

I. INTRODUCTION

THE next generation of wireless communication—5G and beyond—is expected to support cutting-edge, low-latency applications such as autonomous vehicles, immersive augmented reality (AR), and remote medical surgeries [1], [2]. The effective delivery of these services heavily depends on the ability of radio access networks (RANs) to ensure consistent Quality of Service (QoS) while efficiently managing radio spectrum and energy resources [3]. To meet these demands, 5G-compatible radio and baseband processing units, commonly referred to as gNBs, are increasingly embedding Artificial Intelligence (AI) models that enable dynamic traffic handling and intelligent resource allocation. Leveraging the extensive data generated by edge devices, RANs can refine operations using adaptive learning mechanisms [4].

The Open Radio Access Network (O-RAN) architecture has emerged as a transformative approach, offering flexibility, intelligence, and efficiency to fully unlock the potential of 5G New Radio (NR), as outlined by 3GPP and 5GPPP standards [5]. A pivotal component of this architecture is the Radio Intelligent Controller (RIC), which incorporates advanced machine learning techniques through standardized interfaces and the Radio Network Information Base (RNIB) to optimize network performance [2].

One of the most promising machine learning techniques in this architecture is Federated Learning (FL), a decentralized approach that enables training machine learning models across distributed devices or servers without transferring raw data [6]. A hierarchical variant of FL, known as Hierarchical FL (HFL), is particularly well-suited for the mobile-edge-cloud ecosystem [7], [8], [9]. When integrated with the layered structure of O-RAN, HFL enhances network performance, reduces resource consumption, and improves the QoS of user equipment (UE) while preserving data privacy [8]. Unlike traditional approaches, FL minimizes communication overhead by eliminating the need to centralize UE data, thus safeguarding user privacy. Advanced techniques such as MCORANFed [10] and ORANFed [11] have further optimized learning efficiency and resource utilization for single-layer FL in latency-sensitive O-RAN applications. However, these methods do not account for the mobility of local model trainers.

Deploying HFL in O-RAN is further complicated by the dynamic nature of mobile networks. Frequent handovers of UEs between base stations challenge the ability of rApps (applications running on the Non-Real-Time RIC) to manage an ever-changing set of devices during FL model training [4], [12]. Although restarting FL training for a UE post-handover may enhance overall model convergence and efficiency, it introduces delays due to handover execution, potentially increasing the time required to train the global model [13]. This challenge is particularly acute in scenarios involving autonomous vehicles, where wireless resources must be allocated efficiently under stringent latency and mobility constraints [7]. High mobility, interference during handovers, fragmented spectrum, and the increasing number of communication devices further exacerbate these issues [14].

Unlike static networks, managing HFL in O-RAN, as illustrated in Fig. 1, requires addressing unique challenges associated with handover (HO) management [15]. These include: (i) dynamically selecting local trainers for each global round, (ii) deciding whether UEs transitioning to new base stations should continue participating in FL training, (iii) handling UEs that prematurely exit the training process, and (iv) incorporating HO-induced delays into the aggregation algorithm to synchronize local model updates effectively. Retaining all UEs throughout training may enhance model accuracy but significantly prolongs learning time, especially in environments with frequent handovers, such as UAVs or public transit systems. Delays introduced by resuming training at new base stations further slow the overall learning process.

Although recent works [10], [11] propose Non-Real-Time RIC-based frameworks to reduce communication costs and enhance data privacy by localizing information within Near-RT RICs, they do not address the extended learning delays caused by UE handovers across gNB-DUs in hierarchical training. Optimizing HFL training time and resource

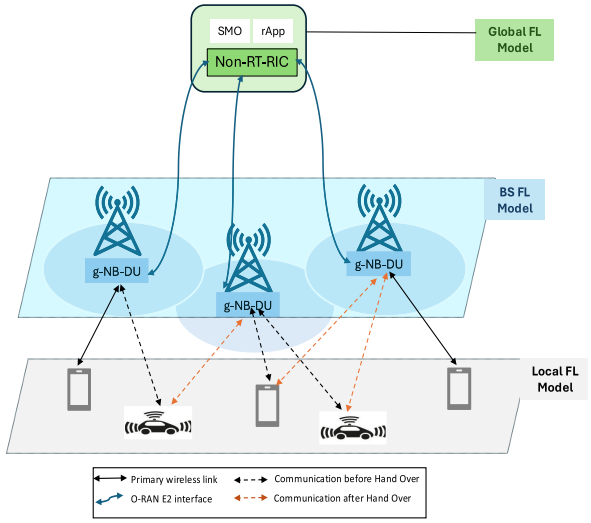

FIGURE 1. Federated Learning model with UE-BS handover and hierarchical aggregation at BS and Non-RT-RIC in O-RAN.

efficiency in the presence of dynamic UE mobility remains a critical and unresolved challenge.

To bridge this gap, this paper presents MHORANFed, an innovative HFL framework that mitigates overall training delay and communication resource costs through the joint optimization of local trainer selection and training resource allocation. Our key contributions are:

- A mathematical formulation of the optimization problem to jointly minimize training time and resource cost in a mobility-aware hierarchical FL framework for O-RAN;
- The development of MHORANFed, a novel algorithm designed to accommodate UE mobility within a hierarchical learning paradigm;
- A thorough convergence analysis of the proposed method, providing insights into solving the underlying non-convex optimization problem;
- Comprehensive simulations that demonstrate the effectiveness of MHORANFed compared to state-of-the-art approaches.

To the best of our knowledge, this is the first work to address the impact of soft inter-gNB-DU handovers on local trainers during HFL training. The remainder of this paper is organized as follows: Section II reviews related work, Section III presents the system model, Section IV describes the proposed approach, Section V provides simulation results, and Section VI concludes with directions for future research.

II. RELATED WORKS

Prior studies [20], [21] have highlighted the unique characteristics and challenges of Federated Learning (FL) architectures, offering comprehensive overviews of existing approaches. The deployment of FL in O-RAN has been explored in works such as [22] and [23], with particular

TABLE 1. Comparison with related literature on FL.

Work	System Model Participants	FL Performance Objective(s)	Hierarchical FL	FL Resource Allocation	Hand Over of UEs over BSs	Convergence Analysis
[16]	BS, UE, Remote cloud	Model Loss, Delay	✓	✓	✗	✓
[17]	UE, BS (RIC)	compute acceleration	✗	✗	✗	✗
[18]	UE, BS, Cloud Server	Data Distribution, Delay	✓	✓	✗	✓
[10]	O-RAN RICs	Resource Cost, Learning Time	✗	✓	✗	✓
[8]	BS, UE, Cloudlets	Resource Cost	✓	✓	✗	✓
[7]	Vehicles, BS, RSU, Cloud Server	Robust Model Aggregation	✓	✗	✗	✓
[19]	UEs, Edge, Cloud Server	Convergence Accuracy	✓	✗	✗	✓
Our Work	**O-RAN RIC BS, UE**	**Learning Time, Resource Usage Cost**	✓	✓	✓	✓

attention to the open, software-defined, virtualized, and intelligent design of the architecture.

The challenge of imbalanced data distributions and learning latency in Hierarchical FL (HFL) across wireless multi-cell networks is addressed in [18]. This work proposes joint user association and wireless resource allocation algorithms for both IID and non-IID data, demonstrating improvements in convergence rates and learning accuracy. In contrast, [17] investigates FL deployment in decoupled O-RAN architectures to enhance computing capabilities. By enabling collaboration among Mobile Virtual Network Operators (MVNOs) for FL model training, it reduces the cost of data collection while boosting performance.

A robust HFL framework tailored to the Internet of Vehicles (IoV) is presented in [7], which counters poisoning attacks through a reputation-based aggregation strategy and logarithmic normalization, offering enhanced robustness. Similarly, [8] optimizes worker aggregator placement and User Equipment (UE) assignment in Mobile Edge Computing (MEC) networks. Its proposed optimization framework and approximation algorithm substantially reduce FL implementation costs, as demonstrated through simulations and real-world testbeds.

To address communication delays between edge and cloud servers, [16] introduces a delay-aware HFL method that applies multiple stochastic gradient descent iterations alongside an adaptive control algorithm, achieving faster global model convergence and reduced resource consumption. In addressing mobility-related performance degradation, [19] proposes a cluster-based HFL approach. More recently, [24] introduced a Reinforcement Learning (RL)-based client selection mechanism that adapts FL training to dynamic environments.

Collectively, these studies tackle key challenges of FL implementation in 5G and beyond Radio Access Network (RAN) environments. Their use cases span resource optimization, hierarchical architectures, and resilience against adversarial threats. However, none of these works address the critical challenge of training HFL models under dynamic handover (HO) conditions—an increasingly common scenario in mobile networks. This gap is especially pressing for high-mobility applications spanning terrestrial, aerial, and underwater domains, where rapid and reliable decision-making is vital.

To fill this gap, we propose MHORANFed, a novel framework that explicitly incorporates HO dynamics into the HFL training process. Table 1 presents a detailed comparison between MHORANFed and existing state-of-the-art HFL and FL frameworks implemented in O-RAN and edge-cloud systems.

III. SYSTEM MODEL

We consider a hierarchical O-RAN system disaggregated into Open Radio Unit (O-RU) at BS, Open Distributed Unit (O-DU) provided close to BS as gNB-DU, and Open Control Unit (O-CU) that controls multiple O-RUs and O-DUs. O-CU control plane (O-CUCP), as a separate entity from O-CU user plane (O-CUUP), monitors the performance KPIs of each UEs via their corresponding BSs. An r-App placed in Non-RT-RIC layer of O-RAN executes the FL training globally

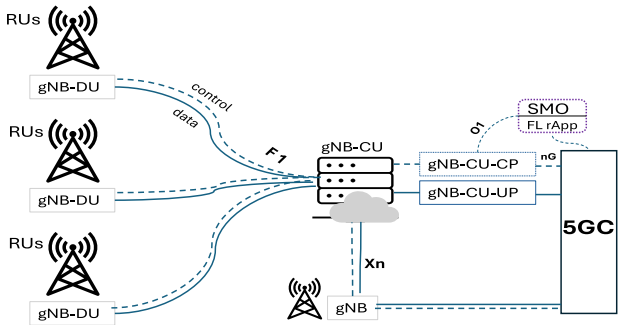

FIGURE 2. System components and standard interfaces in O-RAN.

across the multiple BSs as illustrated in Fig. 2. In each time slot, four operations are implemented to train an FL model: (1) At the UE level, locally collected raw data by the UEs are processed, (2) the model update parameters such as gradients are uploaded at respective BSs for local aggregation, (3) some of the UEs are handed over from one BS to another, and (4) global model update parameters from all the BSs are aggregated at the Non-RT-RIC.

The system consists of a set $\mathcal{N} = \{1, 2, ..., N\}$ of Base Stations (BS) each of which is associated with a gNB-DU. Please note that in this paper, the term BS is used interchangeably with gNB-DU since they are positioned together as depicted in Fig. 1. These gNB-DUs have limited processing power. Let $\mathcal{M} = \{1, 2, ..., M\}$ be the set of UEs in this network. The mobility of these devices results in frequent change of its associated BS invoking several HOs. However, a UE is allowed to be connected to a single BS in one time slot. Let $\mathcal{M}_n^t$ be the set of UEs connected with the BS n in the time slot t. The association between an instance of BS and the UEs follow O-RAN hierarchical definition, which can be modeled as $\sum_{n\in\mathcal{N}} \zeta_{nm} \leq 1 \quad ; \forall m \in \mathcal{M}$. All the UEs participate in model training through FL using their available computational power on a pay per usage cost basis. In this model, we consider a generalized notion of cost that can be specified for a particular type of cost such as energy, battery consumption, etc. Further, all the BSs are connected with an instance of Non-RT-RIC in the Service and Management Orchestration (SMO) layer of O-RAN via a fiber link serving as the E2 interface of O-RAN. This dedicated link is separated from the data plane of Open Control Unit (O-CU). The Non-RT-RIC is hosted on a VM on pay per usage cost basis.

A. HIERARCHICAL FEDERATED LEARNING IN O-RAN

In such a hierarchical federated learning model, the UEs are local trainers, the BSs are the edge model aggregators, and the Non-RT-RIC is the global model aggregator. Model update parameters are exchanged between the UEs and its associated BS periodically during the FL model training as in the traditional FL structure named FedAvg [6]. For the sake of distinction, we call the model trained at the UEs as local FL models, at the BSs as edge FL models, and at the Non-RT-RIC as the global FL model. The aggregated model update parameters from each BS is sent to the Non-RT-RIC after every edge FL model aggregation.

TABLE 2. Summary of key notations.

Notation	System Model Parameters
$\mathcal{M}$	Set of UEs
$\mathcal{N}$	Set of BS (g-NBs)
D_m	Dataset at m^{th} UE
D	Total size of all training data
R^m	Resource usage cost for one local iteration
R_m^{lc}	Total resource cost of local processing at all UEs
R^{bs}	Resource cost for model aggregation at BS
R^{lf}	Resource cost for communication
R^{bs}	Total resource usage cost of HFL
c_m	CPU cycles required to process per bit data
p_m	Processing power of m^{th} UE
p_{tr}	Uniform per unit transmission cost
R_n^g	Backhaul data rate from n^{th} BS to Non-RT-RIC
$F(w)$	Global Model Loss function at the Non-RT-RIC
T_{lc}^m	Local compute latency from m^{th} UE
T_m^n	Transmission delay from m^{th} UE to n^{th} BS
T_{ec}^n	Edge Model aggregation Latency at n^{th} BS
T_m^{HO}	HO execution time for m^{th} UE
$\mathcal{T}_{cost}$	Total HFL model learning time
B_n	Available Bandwidth for allocation at n^{th} BS
Notation	**Input Parameters**
$s(d_m)$	size of the local model vector at m^{th} UE
θ	Local Accuracy
ϵ	Prefixed global accuracy
ρ	Pareto parameter
$H_m^{n\to n'}$	Binary Hand Over (HO) parameter
L	Number of local iterations per global round
G	Number of global rounds
Notation	**Decision Variables**
x_m^g	Participation of m^{th} UE in g^{th} global round
a_m^n	Association of m^{th} UE with BS n
b_m	Bandwidth fraction allocation

Let $F(\mathbf{w})$ be the loss function of the global FL model. To obtain the optimized model $\mathbf{w}^*$, we perform iterative gradient descent method to minimize $F(\mathbf{w})$ over the model vector $\mathbf{w}$. At each BS, the loss function value of an edge FL model is calculated by aggregating its local model updates. Let $fm^t(w)$ be the loss function of the local FL model associated with UE m and $fn^t(w)$ be the loss function of the edge FL model associated with BS n at time slot t. Then,

$$F^t(\mathbf{w}) = \frac{1}{N}\sum_{n=1}^{N} f_n^t(w), \tag{1}$$

where

$$f_n^t(w) = \frac{1}{M}\sum_{m=1}^{M} f_m^t(w). \tag{2}$$

1) UE-BS EDGE MODEL

At time slot t, the UEs serving as local trainers, process their individual raw data. Let $\mathcal{D}_m$ represent the dataset of UE m. To reduce communication overhead, instead of uploading the local model after every local iteration, the model parameters

are uploaded to the associated BS only after every L rounds of local iterations. Let w_m^L denotes local FL model of m^{th} UE at L local iterations. Then the model update equation is:

$$w_m^L = w_m^{L-1} - \eta \nabla f_m(w_m^{L-1}); \forall m \in \mathcal{M}, \tag{3}$$

where η is the learning rate. The model update aggregation in each time slot at the n^{th} BS is performed as:

$$w_n^L = \frac{|\mathcal{D}_m|}{\mathbf{D}} \sum_{m \in \mathcal{M}_n} w_m^L; \forall n \in \mathcal{N}, \tag{4}$$

where $\mathbf{D} = \sum_{m \in \mathcal{M}_n} |\mathcal{D}_m|$.

2) BS – NON-RT-RIC GLOBAL MODEL

After each edge model aggregation, the BS sends its updated model to the Non-RT-RIC. The Non-RT-RIC receives the updated model from each BS and then aggregates as per the following rule:

$$w^G = \frac{1}{N} \sum_{n \in \mathcal{N}} w_n^L; \forall n \in \mathcal{N}, \tag{5}$$

The global model is aggregated after every L local iterations and then communicated back to all the BS nodes. This process is called global round of FL model training.

B. BASE STATION ASSOCIATION AND BANDWIDTH ASSIGNMENT

The channel gain ($C_{m,n}^k(t)$) between a UE m and BS n in a particular time slot t for the radio Resource Block (RB) k is determined by two factors: large scale fading component ($l_{m,n}(t)$) and small scale fading component ($h_{m,n}^k(t)$). While the large scale fading is regulated by the distance between a UE and the corresponding BS it is connected to during one time slot and remains unchanged within this time slot, the small scale fading component is regulated by the variation between two contiguous time-slots. These time-varying components are related as:

$$C_{m,n}^k(t) = l_{m,n}(t)|h_{m,n}^k(t)|^2. \tag{6}$$

Co-channel interference may also occur when the same RB is allocated to multiple UEs. Therefore, as calculated in [22], let $\delta m, n^k(t)$ be the SINR at UE m from BS n in RB k then its uplink spectrum efficiency for time slot t can be given by

$$r_{m,n}(t) = log_2(1 + \delta_{m,n}^k(t)). \tag{7}$$

We define a binary variable a_m^n to denote the association of user m with BS n.

$$a_m^n = \begin{cases} 1 & if\ UE\ m\ is\ associated\ with\ BS\ n, \\ 0\ , & otherwise. \end{cases}$$

Let B_n be the available bandwidth for communicating the FL model training tasks of the associated UEs at the BS n. We define a decision variable $b_m^n(t) \in (0, 1) \subset \mathbb{R}$ to denote the fraction of bandwidth of BS n allocated to the UE m within time slot t. Therefore, the instantaneous data rate between UE m and BS n in time slot t can be given as:

$$R_m^n(t) = a_m^n.b_m^n(t).B_n.r_m^n(t) \tag{8}$$

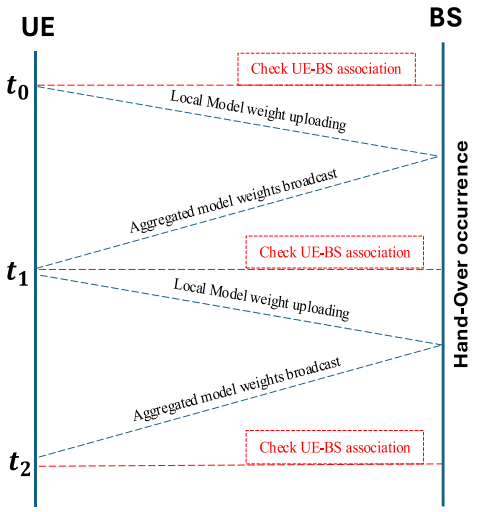

FIGURE 3. Sequence of steps among the HFL training nodes in every communication round.

C. INTER gNB-DU HANDOVER

We consider a soft handover in which the source and destination cells are associated with different gNB-DUs while the 5G core (5GC), which makes the HO decision, remains the same as illustrated in Fig. 2. This definition follows the technical specification of [25] which is also analysed by [26] and [27]. In terms of physical deployment, the User Plane Function (UPF) of the 5GC can either be moved within the same UPF instance (intra-UPF) or across different UPF instances (inter-UPF). Although there is a dedicated m-Plane (defined in the O-RAN specifications) for such network management operations, this conditional inter-gNB-DUs handover results in change of associated UEs temporarily. In turn, this leads to fluctuations in channel gains and the BS throughput. Consequently, the bandwidth allocation of the updated UEs changes. A binary handover parameter $Hm^{n \to n'}$ indicates whether UE m is handed over from BS n to BS n'.

$$Hm^{n \to n'} = \begin{cases} 1 & if\ HO\ occurs\ from\ BS\ n\ to\ BS\ n', \\ 0\ , & otherwise\ (No\ HO). \end{cases}$$

Following the HO, the resulting association of a UE with a BS will also change and hence the effective data transmission rate changes. So, the updated subset of the UEs becomes $\mathcal{M}_{n'}(t)$ instead of $\mathcal{M}_n(t)$. Moreover, since the HO occurs during an ongoing model training, an overhead of handover time also needs to be accounted in the total FL training time. The FL rApp (located in the O-RAN SMO) records this HO event and calculates the time elapsed in rejoining the UE back into the FL model training. Let T_m^{HO} be the time elapsed in the handover execution of UE m. T_m^{HO} consists of internal delay caused by measurement reports exchange, TTT (Time-To-Trigger) parameters, etc. It should be noted that T_m^{HO} also includes delay arising from channel interference caused by high mobility of UEs in the adjacent BS.

D. HFL RESOURCE MODEL

The FL model training incurs compute and communication resources consumption. In the first layer of HFL, training local FL model requires UE's compute resource, and bandwidth is required between the UEs and the corresponding BS for transmitting the model parameters.

1) COMPUTE RESOURCE

Let $s(D_m)$ be the size of the raw dataset to be processed at m^{th} UE, p_m be its processing power in cycles/sec, and c_m be the CPU cycles per bit to process the data. Then, the resource usage cost for one local iteration is given by:

$$R_m = s(D_m).c_m.(p_m)^2 \tag{9}$$

So, for L local iterations, the computation cost for UE m is $L.R_m$. Now, at the BS level, model parameters' aggregation is performed after every L local iterations (i.e., or a global round G). Naturally, $G.k = L$, meaning the total number of local rounds is always a whole number multiple of the number of global iterations. Therefore, the total resource cost of the HFL required for the local processing at all UEs is given by:

$$R^{lc} = G.\sum_{m\in\mathcal{M}} L.R_m \tag{10}$$

Further, let $s(d_m)$ be the size of the model parameters from the m^{th} UE. Then, at the BS level, the resource usage cost required for processing the local FL model aggregation is:

$$R^{bs} = \sum_{m\in\mathcal{M},n\in\mathcal{N}} G.s(d_m).p_n \tag{11}$$

The compute resource usage cost at the Non-RT-RIC is negligible as the processing power there is not scarce. So, we do not model that part.

2) COMMUNICATION RESOURCE

Wireless resources are consumed for transmitting the model updates from UEs to their associated BS. Therefore, the communication resource usage cost incurred by the local FL model is given by:

$$R^{lf} = G.\sum_{m\in\mathcal{M}}\sum_{n\in\mathcal{N}} a_m^n.b_m^n.B_n.r_m^n.p_{tr} \tag{12}$$

where, $p_{tr} \in \mathbb{R}^+$ is the uniform per unit bit transmission cost. The communication resource usage cost between BS and the Non-RT-RIC is comparatively negligible as it is provided by the non-scarce backhaul fiber link. Hence, the overall resource usage cost of this HFL can be summed up as;

$$\mathcal{R}_{cost} = R^{lc} + R^{bs} + R^{lf} \tag{13}$$

E. LEARNING TIME MODEL

Due to the limited resources in UE-BS layer, both compute and transmission latency are the main performance factors. These latency occur at both the layers of HFL.

1) UE-BS EDGE LAYER

In this layer, the latency consists of local model processing at each participating UE and model parameters uploading by all of them to the respective BSs. The local compute latency can be modelled as:

$$T_m^{lc} = \frac{s(D_m).c_m}{p_m}. \tag{14}$$

Since a BS will have to wait for all its participating UEs to receive the model update before it can start the aggregation, the effective compute latency at BS n over all its UEs in time slot t is given by:

$$\max_{m\in\mathcal{M}_n(t)} \{T_m^{lc}\}. \tag{15}$$

Further, the delay in its model parameters' transmission to the corresponding temporal BS n can be modelled as:

$$T_m^n = \frac{s(d_m)}{R_m^n(t)}. \tag{16}$$

2) BS–NON-RT-RIC LAYER

In this layer, the local FL model aggregation at BS and the global FL model aggregation at the Non-RT-RIC incur compute delays whereas the model parameters exchange adds transmission delay. A wired backhaul, i.e., a dedicated fiber link can be used for this communication, which offers a much higher speed than the wireless links between BSs and UEs. However, due to the straggler effect of FL training, the synchronous model aggregation may become a significant part of the learning time. Because of the model integrity, the size of the model parameters remain the same after the aggregation. Let $s(d)$ be the size of this model update and p_n be the processing power in bit per sec of the VM associated with the n^{th} BS. Then, the time required for processing the model is:

$$T_n^{ec} = \frac{s(d)}{p_n}. \tag{17}$$

The delay of transmitting the model from the n^{th} BS to the Non-RT-RIC is:

$$T_n^g = \frac{s(d)}{R_n^g}, \tag{18}$$

where R_n^g is the backhaul data rate from the n^{th} BS to the Non-RT-RIC. Since the Non-RT-RIC aggregates the model in the core network where compute resource is not scarce, the corresponding compute delay is negligible. Therefore, the overall learning time of this HFL can be summed up as:

$$\mathcal{T}_{cost} = \max_{m\in\mathcal{M}_n}\left\{H_m^{n\to n'}.T_m^{HO} + T_m^{lc} + T_m^n\right\} + \max_{n\in\mathcal{N}}\left\{T_n^{ec} + T_n^g\right\} \tag{19}$$

F. PROBLEM FORMULATION

We define x_m^g a binary variable that decides whether the m^{th} UE which has been handed over from one BS to another will continue to take part in the g^{th} global round of HFL training or it will be dropped out of this particular round.

$$x_m^g = \begin{cases} 1\ ; & \textit{if } m^{th} \textit{ UE takes part in } g^{th} \textit{ global round}, \\ 0\ ; & \textit{otherwise}\ . \end{cases}$$

While a handed over UE may contribute to the global model in terms of accuracy, data heterogeneity, and convergence, it also increases the overall model learning time because of the time elapsed in handover and resuming the model update. In our proposed architecture, a rApp running in the Non-RT-RIC monitors the accuracy of the in-training model and the elapsed learning time following the completion of every global round to make the decision of accepting such UEs in the FL training as depicted in Fig. 3. The objective of this system is to minimize the compute and communication costs and the training latency of all the participating UEs over the required global rounds, which is modeled as follows:

$$cost(t) = \sum_{m\in\mathcal{M}} x_m^g \Big\{ \sum_{n'\in\mathcal{N}} \sum_{m\in\mathcal{M}_{n'}(t)} H_m^{n\to n'}.T_m^{HO} + \sum_{n\in\mathcal{N}} \sum_{m\in\mathcal{M}_m(t)} (\rho.\mathcal{T}_{cost} + (1-\rho).\mathcal{R}_{cost}) \Big\} \quad (20)$$

The first term of this cost function represents the delay incurred solely due to HO execution, while the second term captures the training delay along with the associated resource usage cost. Notably, the impact of HO execution delay also extends to the second term, resulting in a compounded effect on the overall cost function. This function serves as the objective function for the subsequent optimization problem.

$$\min_{\mathbf{x},\mathbf{a},\mathbf{b}} \sum_{t=1}^{G} cost(t) \quad (21)$$

subject to:

$$\sum_{m\in\mathcal{M}_n} a_m^n(t).b_m^n(t) \le 1;\ \forall n\in\mathcal{N}, t=\{1,2,...,G\}, \quad (21a)$$

$$\sum_{m\in\mathcal{M}_n}^{M} b_m^n(t) = 1;\quad \forall n\in\mathcal{N}, \quad (21b)$$

$$\sum_{n\in\mathcal{N}} a_m^n(t) = 1;\quad \forall m\in\mathcal{M}_n, \quad (21c)$$

$$\sum_{n,n'\in\mathcal{N}} a_m^n(t).H_m^{n\to n'} \le 1\ ;\forall m\in\mathcal{M}, \quad (21d)$$

$$\sum_{m\in M, n\in N} R_m^n(t).x_m^g \le r_{m,n}(t)\ ;\forall g\le G, \quad (21e)$$

$$\sum_{n\in\mathcal{N}} \zeta_{nm} \le 1\ ;\forall m\in\mathcal{M}, \quad (21f)$$

$$a_m^n, x_m^g \in \{0,1\}, \quad (21g)$$

$$b_m^n(t) \in (0,1) \quad (21h)$$

Constraint (21a) guarantees that the sum of bandwidth fractions allocated to all the local trainers does not exceed the available bandwidth at each BS. Constraint (21b) defines the integrity of bandwidth allocation for each BS. Constraint (21c) ensures that a UE is associated with a single BS in each time slot. Constraint (21d) states that a UE can be handed over to a maximum one BS in each time slot. Constraint (21e) denotes that the sum of selected UEs' data rates obtained through the bandwidth allocation must not exceed the spectrum uplink efficiency in any global round. (21f) reflects the association constraint of O-RAN hierarchy. (21g and 21h) are the defining conditions on the decision variables.

Algorithm 1 Recovering Feasible Integer Solution using PCA

Input: Relaxed SDP solution W_m (positive semi-definite matrix)
Output: Approximate integer solution $\hat{x}, \hat{a}, \hat{b}$
Step 1: Compute Principal Components
Compute the eigenvalue decomposition: $W_m = U\Lambda U^T$
Select the top principal component: $v_1 = U[:, 1]$ (corresponding to the largest eigenvalue)
Step 2: Extract Initial Integer Approximation
for each element $v_1(i)$ **do**
    Assign $\tilde{x}_m^g = \text{sign}(v_1(i))$ (Convert to binary by thresholding at 0)
end for
Step 3: Randomized Rounding
for each m, n **do**
    Compute probability $p_m^n = \frac{|v_1(m,n)|}{\sum_{m'}|v_1(m',n)|}$
    Set $\hat{a}_m^n$ as a Bernoulli random variable with probability p_m^n
end for
Step 4: Feasibility Refinement
for each constraint in (21) **do**
    Project the solution onto the feasible set
    Adjust $\hat{a}, \hat{b}, \hat{x}$ using constraint enforcement
end for
Step 5: Return Recovered Integer Solution
return $\hat{x}, \hat{a}, \hat{b}$.

IV. PROPOSED SOLUTION: MHORANFed

The problem (21) is a mixed-integer non-linear programming (MINLP) model. The objective function is non-convex and the constraint (21a) contains bilinear terms (product of decision variables **a** and **b**). Obtaining the exact optimal solution of this NP-Hard problem is intractable with existing mathematical solvers. Nonetheless, Semi Definite Programming (SDP) [28] relaxation is known to provide tight bounds. Therefore, we relax the constraints and the objectives to a convex semi-definite form.

Fig. 4 outlines our proposed solution approach to the joint optimization problem (21) aimed at minimizing the total HFL training cost under bandwidth and handover-aware local trainers' selection constraints. The problem is first reformulated as a SDP problem (22), which is then approximately solved using Algorithm 1 to obtain a feasible solution. Following this, the system performs post-handover local trainer selection and allocates bandwidth among the selected devices. Finally, Algorithm 2 resumes to continue with the learning rounds based on the optimized configuration.

To relax the bilinear term $(a_m^n \cdot b_m^n)$, we introduce a new variable W_m defined as:

$$W_m = \begin{bmatrix} 1 & a_m^n \\ a_m^n & b_m^n \end{bmatrix}, \quad W_m \succeq 0.$$

So, the constraint (21b) transforms to

$$\sum_{m \in \mathcal{M}_n} W_m \leq 1, \quad \forall n \in \mathcal{N}, t = \{1, 2, \ldots, G\}$$

We also relax the binary decision variables into continuous real variables as: $x_m^g \in [0, 1]$, $a_m^n \in [0, 1]$, $b_m^n \in [0, 1]$ to make it solvable through a mathematical solver [29]. Then, a rounding technique is applied to obtain the binary values of these variables. In particular, we performed principal component analysis (PCA) on the obtained matrix *Wm* solution and iteratively adjusted its feasibility as shown in Algorithm 1. The PCA based rounding is preferred over other rounding methods as it offers a principled and computationally efficient way to project high-dimensional approximated solutions onto a lower-dimensional feasible space [30].

A. OPTIMALITY GAP ANALYSIS

The SDP based relaxation leads to a sub-optimal approximation which is a lower bound on the exact solution as can be directly inferred from its definition as follows:

The non-convex bilinear inequality constraint (21a):

$$a_m^n(t) \cdot b_m^n(t) \leq 1$$

is relaxed using a positive semidefinite matrix:

$$W_m^n(t) = \begin{bmatrix} 1 & a_m^n(t) & b_m^n(t) \\ a_m^n(t) & a_m^n(t)^2 & \theta_m^n(t) \\ b_m^n(t) & \theta_m^n(t) & b_m^n(t)^2 \end{bmatrix}, \quad W_m^n(t) \succeq 0$$

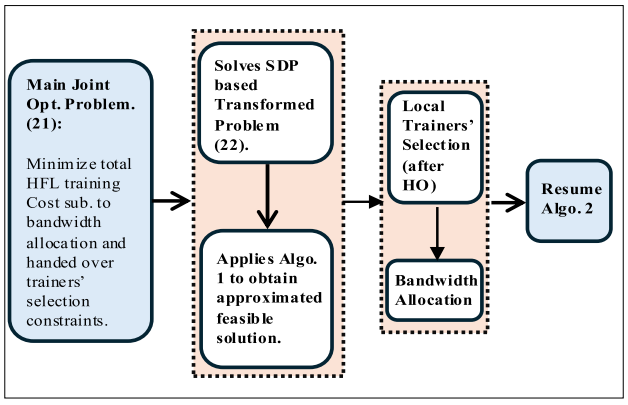

FIGURE 4. Proposed solution schema.

where $\theta_m^n(t)$ serves as a convex surrogate for the product $a_m^n(t) \cdot b_m^n(t)$.

We replace the rank-1 matrix constraint

$$W_m^n(t) = \mathbf{v}_m^n(t)\mathbf{v}_m^n(t)^\top, \quad \text{with} \quad \mathbf{v}_m^n(t) = \begin{bmatrix} 1 \\ a_m^n(t) \\ b_m^n(t) \end{bmatrix}$$

by a relaxed convex constraint $W_m^n(t) \succeq \mathbf{v}_m^n(t)\mathbf{v}_m^n(t)^\top$, allowing $W_m^n(t)$ to lie in the convex hull of rank-1 matrices. This enlargement of the feasible region leads to the SDP:

$$\min_{\mathbf{x},\mathbf{a},\mathbf{b},\mathbf{W}} \sum_{t=1}^{G} \text{cost}(t) \tag{22}$$

$$\text{s.t. } W_m^n(t) \succeq 0, \quad \forall m, n, t \tag{22a}$$

(plus relaxed versions of other constraints from (21))

The optimal value f_{sdp}^* of this convex relaxation satisfies:

$$f_{\text{sdp}}^* \leq f^*$$

where f^* is the optimal value of the original non-convex problem. This is because the relaxed SDP includes all feasible integer points and additional fractional ones, resulting in a lower bound on the true optimum. The gap between f^* and f_{sdp}^* is the optimality gap.

In Lemma 1 of our convergence analysis, we show that under a set of conditions on the model loss functions and its learning rate, this optimality gap lies within the controllable range of convergence.

Using this approximated solution, we design an algorithm called Mobility Aware Hierarchical Federating Learning for O-RAN (MHORANFed). The global training loop iterates until the global model accuracy ($\epsilon \in (0, 1)$) reaches a predefined threshold ϵ^* as outlined in Algorithm (2). By considering the mobility of UEs and the hierarchical structure of O-RAN, MHORANFed aims to achieve efficient and accurate federated learning in dynamic network environments.

By utilizing the optimal set of local trainers associated with a BS and the handed-off UEs allowed back in the model training in each global round, MHORANFed mitigate the bias caused by handover and in favour of the BS having a relatively higher number of local trainers. Moreover, the synchronous communication resulting in the delay calculated as modeled by (15), ensures that the optimal solution has the total learning time with ρ times Pareto importance as defined in (20).

B. COMPLEXITY ANALYSIS

Algorithm 1 consists of two main loops. The outer-loop depends on the number of global rounds (G) having a time complexity of $\mathcal{O}(G)$. According to [31], the MHORANFed performance will be unaffected as long as the convergence time of FL global iterations is upper-bounded by $\mathcal{O}(log(1/\epsilon^*)$, where ϵ^* is the model accuracy. The inner-loop has the complexity of $\mathcal{O}(L)$, where L is the number of local iterations. Let $KSDP$ be the approximated iterations of SDP then $\mathcal{O}(KSDP)$ [28] is the computational complexity of the optimization problem in (21), as drawn in the line 2 of Algorithm 1. Therefore, the overall complexity of MHORANFed is $\{M.\mathcal{O}(L) + N.\mathcal{O}(KSDP)\}.\mathcal{O}(log(1/\epsilon^*))$. Here, $M = |\mathcal{M}|$ is the number of UEs and $N = |\mathcal{N}|$ is the number of BSs.

Algorithm 2 Mobility-aware Hierarchical FL for O-RAN (MHORANFed)

Input:
Untrained global FL model w;
Set of participating UEs $\mathcal{M}$ and BS-gNB servers $\mathcal{N}$;
HO occurrence at concerned UEs $H_m^{n\to n'}$;
Stopping criteria ϵ^*
Output: Trained global HFL model w^*
for each global round $g \le G$ **do** ▷Global rounds
Non-RT-RIC rApp solves (22)
Non-RT-RIC assigns bandwidth $\hat{\mathbf{b}}$ to UEs $\hat{\mathbf{x}}$, $\hat{\mathbf{a}}$.
for Local iteration:1 to L**do** ▷ Local training at UEs
UE m downloads the edge model w_m^{L-1} from its associated BS-gNB.
UE trains local model w_m^L using Equation (3).
BS n aggregates local models to get w_n^L via Equation (4).
end for
BS-gNB servers upload aggregated models to the Non-RT-RIC.
Non-RT-RIC aggregates models to get w^G using Equation (5).
Non-RT-RIC updates global model accuracy.
rApp utilizes $H_m^{n\to n'}$ to update current UE associations.
while $\epsilon \ge \epsilon^*$ **do** ▷Convergence check

C. CONVERGENCE ANALYSIS

Lemma 1 (Boundary of Convergence): If $F(w^*)$ and $F(w^G)$ be the final loss function values corresponding to f^* and f^*_{sdp} i.e. the optimal and the approximated solutions respectively, then

$$f^* - f^*_{\text{sdp}} \ge \mathbb{E}[F(w^G) - F(w^*)]$$

provided the following conditions hold:

- $\eta < \frac{1}{R}$,
- $\eta\mu > 1 - \sqrt[L]{\frac{1}{4M}}$.

Proof: After G global rounds of communication between the Non-RT-RIC and the set of BSs, the expected optimality gap is bounded by:

$$\mathbb{E}[F(w^G) - F(w^*)] \le \beta[F(w^0) - F(w^*)] + (1-\beta)\frac{L\eta p}{4\gamma}$$

where $\gamma = (1-\eta\mu)^L$, and $\beta = \left(\frac{2M\gamma}{L}\right)^G$.

In each round, the left-hand side of the above inequality is governed by two key terms from the SDP-based approximated solution of (21):

- the geometric decay term: $\beta[F(w^0) - F(w^*)]$,
- and the residual error floor: $(1-\beta)\frac{L\eta p}{4\gamma}$.

The term $\beta = \left(\frac{2M\gamma}{L}\right)^G$ depends exponentially on the number of global rounds G, and shrinks rapidly as G increases, provided that:

$$\gamma = (1-\eta\mu)^L < 1$$

This holds true when the learning rate η and the local smoothness constant μ satisfy:

$$\eta\mu > 1 - \sqrt[L]{\frac{1}{4M}}$$

Together, these conditions ensure that:

- the geometric decay dominates initially, reducing the gap quickly,
- the residual floor becomes small with careful tuning of η,
- and the SDP relaxation of the original problem provides a tight lower bound on $F(w^*)$, enabling estimation of the gap:

$$\mathbb{E}[F(w^G) - F(w^*)] \le f^* - f^*_{\text{sdp}}$$

Hence, this theoretical bound directly connects the choice of algorithmic parameters to the rate of convergence and the quality of the approximate solution.

Theorem 1 (UE-BS Edge Layer): Assuming the global loss function $F(w)$ to be R-smooth and μ-strongly convex (true for the standard FL convergence analysis [32], and that each UE performs L local updates before uploading its updated model weights to the corresponding BS, if the following conditions are satisfied:

- $\eta < \frac{1}{R}$,
- $\eta.\mu > 1 - \sqrt[L]{\frac{1}{4M}}$,
- $F(w^o) - F(w^*) > \frac{L.M.p}{4.(1-\eta.\mu)^L}$,

then we have:

$$\begin{cases} \frac{2M}{L}(1-\eta\cdot\mu)^L \in (0,1), \\ \mathbb{E}[F(w^L) - F(w^*)] \le (1-\eta\cdot\mu)^L[F(w^0) - F(w^*)] \\ + \frac{L\cdot\eta\cdot p}{2} \end{cases} \tag{23}$$

where w^L denotes the model weights after L rounds of local updates and w^o denotes the initial weight parameter.

Proof: We derive the convergence of L local updates first. By utilising the assumptions of strong convexity and smoothness for each local update $l \in 1, 2, \ldots L$, we have:

$$\begin{aligned} &\mathbb{E}[F(w^l) - F(w^*)] \\ &\le F(w^{l-1}) - F(w^*) \\ &\quad - \eta\mathbb{E}[< \nabla F(w^{l-1}), \nabla f(w^{l-1}; q_l) >] \\ &\quad + \frac{L\eta^2}{2}\mathbb{E}[||\nabla f(w^{l-1}; q_l)||^2] \\ &\le F(w^{l-1}) - F(w^*) - \frac{\eta}{2}||\nabla F(w^{l-1})||^2 \\ &\quad + \frac{\eta}{2}\mathbb{E}[||\nabla F(w^{l-1}) - \nabla f(w^{l-1}; q_l)||^2] \\ &\le F(w^{l-1}) - F(w^*) - \frac{\eta}{2}||\nabla F(w^{l-1})||^2 \\ &\quad + \frac{\eta p}{2} \quad \text{(using the graded variance)} \\ &\le F(w^{l-1}) - F(w^*) - \eta\mu[F(w^{l-1}) - F(w^{)}] + \frac{\eta p}{2} \\ &\le (1-\eta\mu)[F(w^{l-1}) - F(w^*)] + \frac{\eta p}{2} \end{aligned} \tag{24}$$

This gives us a convergence bound for each local iteration $l \in 1, 2, ..., L$. By extending this for all the local updates and telescoping, we have after L local updates:

$$\begin{aligned}
&\mathbb{E}[F(w^L) - F(w^*)] \\
&\leq (1-\eta\mu)[F(w^{L-1}) - F(w^*)] + \frac{\eta p}{2} \\
&\leq (1-\eta\mu)[(1-\eta\mu)[F(w^{L-2}) - F(w^*)] \\
&\quad + \frac{\eta p}{2}] + \frac{\eta p}{2} \\
&\ldots\ldots\ldots \textit{by telescoping with eq. (24)} \\
&\leq (1-\eta\mu)^L[F(w^0) - F(w^*)] + \\
&\frac{\eta p}{2}\sum_{l=1}^{L}(1-\eta\mu)^{l-1} \\
&\leq (1-\eta\mu)^L[F(w^0) - F(w^*)] + \\
&\frac{\eta p}{2}\frac{1-(1-\eta\mu)^L}{1-(1-\eta\mu)} \\
&\leq (1-\eta\mu)^L[F(w^0) - F(w^*)] + \\
&\frac{\eta p}{2}\frac{L\eta\mu}{1-(1-\eta\mu)} \\
&\leq (1-\eta\mu)^L[F(w^0) - F(w^*)] + \frac{L\eta p}{2} \qquad (25)
\end{aligned}$$

At the Non-RT-RIC, the concerned FL Manager rApp performs global model aggregation after every m updated model weights at time-slot t.

Following it we have: $w^t = \frac{L}{M}\sum_{i=1}^{\frac{M}{L}} w_i^L$, where w_i^L denotes the local model update in the i^{th} UE after L local iterations.

Theorem 2 (BS-Non-RT-RIC Layer): After G global rounds between the Non-RT-RIC and the set of BSs, the convergence bound of MHORANFed is:

$$\mathbb{E}[F(w^T) - F(w^*)] \leq \beta[F(w^0) - F(w^*)] + (1-\beta)\frac{L\eta p}{4\gamma} \qquad (26)$$

where $\gamma = (1-\eta\mu)^L$, *and* $\beta = (\frac{2M\gamma}{L})^G$.

Proof: Following the definition of the weight update rule of w^t for every global round, we have:

$$\begin{aligned}
&\mathbb{E}[F(w^t) - F(w^*)] \\
&\leq \frac{L}{M}\sum_{i=1}^{M/L}[F(w_i)^L - F(w^*)] \\
&\leq \frac{L}{M}\sum_{i=1}^{M/L}[(1-\eta\mu)^L(F(w_i) - F(w^*)) + \frac{LMp}{2}] \\
&\leq \frac{M}{L}[(1-\eta\mu)^L(F(w^0) - F(w^*)) + \frac{L\eta p}{2}] \\
&\leq \frac{M}{L}[(1-\eta\mu)^L(F(w^0) - F(w^{t-1}) \\
&\quad + F(w^{t-1}) + F(w^*)) + \frac{L\eta p}{2}] \\
&\leq \frac{M}{L}(1-\eta\mu)^L(F(w^0) - F(w^{t-1})) \\
&\quad + \frac{M}{L}(1-\eta\mu)^L(F(w^{t-1}) - F(w^*)) + \frac{ML\eta p}{2} \\
&\leq \frac{M}{L}(1-\eta\mu)^L(F(w^{t-1}) - F(w^*)) \\
&\quad + \frac{M}{L}(1-\eta\mu)^L(F(w^{t-1}) - F(w^*)) + \frac{ML\eta p}{2} \\
&\leq (\frac{2M}{L}(1-\eta\mu)^L)[F(w^{t-1}) - F(w^*)] + \frac{ML\eta p}{2} \qquad (27)
\end{aligned}$$

Therefore, the after G global rounds, the convergence bound comes down to:

$$\begin{aligned}
&\mathbb{E}[F(w^G) - F(w^*)] \\
&\leq (\frac{2M}{L}(1-\eta\mu)^L))[F(w^{G-1}) - F(w^*)] + \frac{ML\eta p}{2} \\
&\ldots\ldots \textit{telescoping by eq.(27)} \\
&\leq (\frac{2M}{L}(1-\eta\mu)^L))^G[F(w^0) - F(w^*)] \\
&\quad + \frac{(1-\frac{2M}{L}(1-\eta\mu)^L)^G ML\eta p}{2(1-\frac{2M}{L}(1-\eta\mu)^L)} \\
&\leq (\frac{2M}{L}(1-\eta\mu)^L)^G[F(w^0) - F(w^*)] \\
&\quad + \frac{(1-\frac{2M}{L}(1-\eta\mu)^L)^G ML\eta p}{\frac{4M}{L}(1-\eta\mu)^L)} \\
&\leq (\frac{2M}{L}(1-\eta\mu)^L)^G[F(w^0) - F(w^*)] \\
&\quad + \frac{L\eta p}{4(1-\eta\mu)^L}.(1-(\frac{2\eta}{L}(1-\eta\mu)^L)^G) \qquad (28)
\end{aligned}$$

To simplify eq. (28), replacing $\gamma = (1-\eta\mu)^L$ and $\beta = (\frac{2M\gamma}{L})^G$. Then, we have:

$$\mathbb{E}[F(w^T) - F(w^*)] \leq \beta[F(w^0) - F(w^*)] + \frac{L\eta p}{4\gamma}(1-\beta) \qquad (29)$$

V. NUMERICAL RESULTS AND ANALYSIS

A. SIMULATION SETTINGS

We simulate 5 BSs and 100 UEs randomly in a distributed coverage region. At the beginning, a random subset of 20 UEs are connected to each BS such that the load of all BSs are balanced in terms of the bandwidth required for model update parameters' transmission. After the completion of 20, 40, and 70 global rounds, a subset of 5, 3, and 6 UEs respectively opt for HO to their nearest BS. A similar occurrence of HO is set in the experiment for a total of 10 times and the average performance of MHORANFed is plotted to counter the randomness bias. A wireless channel model between the UEs and the respective BSs is considered with both small and large scale fading components. We set the path loss model of $128.1 + 37.6log_{10}(d)$ for the large scale fading and set Rayleigh distribution for the small scale fading. The processing power of UEs is set uniformly in the range from 1.0 GHz to 2.5 GHz and that of BSs is in the range from 2.0 GHz to 3 GHz. Uplink bandwidth capacity is 50 MHz for each BS. For the second layer of the HFL, the available fiber bandwidth is 20 MHz.

TABLE 3. Simulation parameters.

Parameter	Value
System Model Parameters	
Number of BSs	5
Number of UEs	100 (random placement)
Initial UE-BS Association	20 UEs per BS (balanced load)
HO Events	After 20, 40, 70 rounds: 5, 3, and 6 UEs switch
HO Repetitions	10 runs (average results)
Channel Model	Small- and large-scale fading
Path Loss Model	$128.1 + 37.6 \log_{10}(d)$
Fading Type	Rayleigh
UE CPU	$\sim \mathcal{U}(1.0, 2.5)$ GHz
BS CPU	$\sim \mathcal{U}(2.0, 3.0)$ GHz
Uplink Bandwidth	50 MHz per BS
Fiber Bandwidth	20 MHz (2nd HFL layer)
Loss Function	Cross-Entropy (Non-convex), Mean Square Error (Convex)
Input Parameters (Datasets and Accuracy)	
CIFAR-10	50k train, 10k test
MNIST	60k train, 10k test
Network Traffic	160k train, 40k test
Data Allocation	IID and non-IID across UEs
$\epsilon^*_{\text{MNIST}}$	93% (CNN), 91% (SVM)
$\epsilon^*_{\text{CIFAR-10}}$	78% (CNN), 81% (SVM)
$\epsilon^*_{\text{Traffic}}$	90% (LSTM)

The standard CIFAR-10 dataset [33] consisting of 50,000 training images and 10,000 train images and the MNIST dataset [34] containing 60,000 training and 10,000 test images are adopted for the multi-class classification problem. These datasets are distributed onto all 100 UEs with skewed class labels to represent non-IID scenario and uniformly using stratified sampling method to represent IID scenario at the FL training initialization. The stopping criteria for MNIST, defined as the model accuracy ϵ^*, is set as 93% which is obtained through centralized ML model training with a 2 layer CNN model and 91% model accuracy with SVM. The ϵ^* for CIFAR-10 is 78%, as obtained through centralized CNN model with 2 layers and 81% with SVM. A time series dataset taken from [35] is also processed for predicting network traffic. The categorical cross-entropy is the loss function for the classification problem while the Mean Square Error (MSE) is the loss function for the traffic prediction problem.

We trained the models under two different dataset distributions to incorporate the impact of data heterogeneity. (i) IID case: the whole train and test dataset as described above us uniformly distributed across the associated local trainers. We also employ stratified sampling to maintain a proportional class label distribution for the MNIST and CIFAR-10 dataset. Similarly, we maintain the same time duration for the traffic volume dataset. (ii) Non-IID case: we utilized skewed class distribution for the image classification task and non-uniform time-span distribution for the traffic prediction task.

B. BASELINES

The following baseline schemes are implemented for this comparative performance analysis:

- **'All-Dropped':** This scheme excludes all the UEs which undergo HO in HFL.
- **'MHORANFed':** The near optimal solution obtained through our proposed algorithm in this paper.

TABLE 4. Number of global communication rounds to achieve the target accuracy with different pareto Trade-offs and learning rates.

		Number of Global FL Rounds					
Dataset	**Method**	ρ=0.5 η=0.01	ρ=0.5 η=0.05	ρ=0.01 η=0.01	ρ=0.01 η=0.05	ρ=0.99 η=0.01	ρ=0.99 η=0.05
CIFAR-10	All-Dropped	114	116	112	115	118	117
	MHORANFed	**101**	**102**	**103**	**100**	**104**	118
	Random	113	115	110	114	116	119
	HFL-0	112	114	108	113	117	115
	DFL	110	117	111	116	115	**110**
	MACFL	109	113	110	112	114	116
	FedPPO	108	111	109	110	113	114
MNIST	All-Dropped	133	130	127	134	132	131
	MHORANFed	**113**	**115**	**114**	**116**	126	**117**
	Random	129	128	125	132	130	129
	HFL-0	124	126	121	128	129	128
	DFL	126	131	123	130	128	127
	MACFL	121	127	122	129	127	125
	FedPPO	119	123	120	124	**119**	122
Traffic	All-Dropped	56	55	52	53	58	57
	MHORANFed	**39**	**40**	43	**41**	**36**	46
	Random	50	51	48	49	54	53
	HFL-0	47	49	46	48	52	50
	DFL	44	53	45	50	51	54
	MACFL	42	46	**38**	47	49	51
	FedPPO	41	44	42	45	47	**42**

- **'Random':** In this scheme, a random set of UEs are selected consisting of one or more handed over UEs and dropped UEs.
- **'HFL-0':** This is the algorithm derived from [18] and adapted to suit the comparable framework in this paper. In this variant of HFL, UEs' handovers are not considered.
- **'DFL':** This is a delay aware HFL [16] having sub-linear convergence rate and no consideration of handovers.
- **'MACFL':** Taking into account the impact of users' mobility on the FL training in wireless networks, MACFL (Mobility-Aware Cluster FL) [19] serves as the closest baseline.
- **'FedPPO':** We trained a reinforcement learning (RL) based client selection strategy for the hierarchical FL by utilizing Federated Proximal Policy Optimization (FedPPO) [24].

C. KEY METRICS

The main metrics used for comparison are as follows.

- **Convergence:** This fundamental property assesses an FL method's ability to attain the threshold performance over the number of global rounds. A higher convergence rate results in a smaller number of global rounds as it directly translates to lower training time. We compare the convergence rate of all the baselines for both types of learning tasks over the IID and non-IID cases.
- **Training Cost:** As defined in (21), there are two main components of the training cost: i) learning time shich is the total time taken to train the final global model,

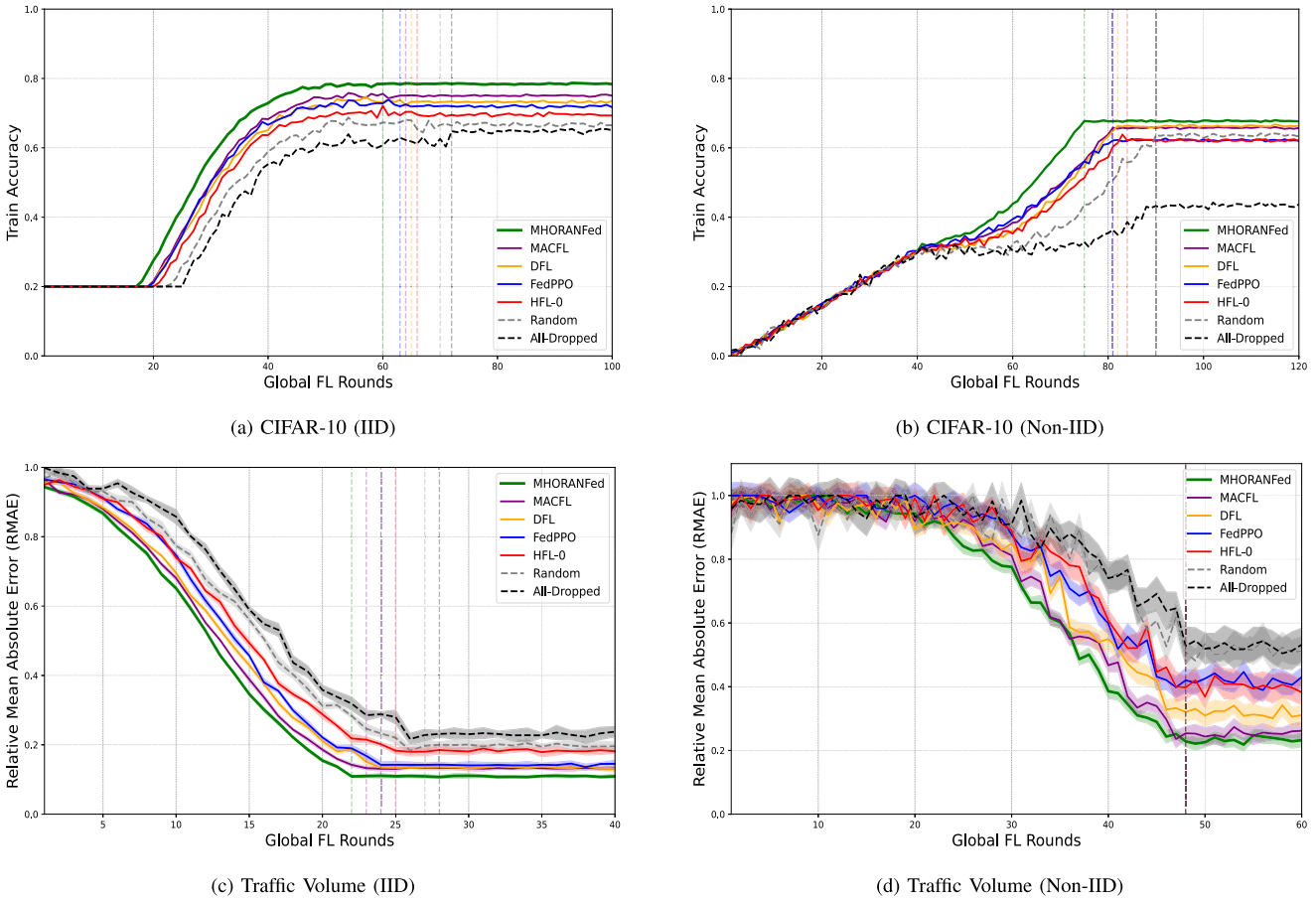

(a) CIFAR-10 (IID)

(b) CIFAR-10 (Non-IID)

(c) Traffic Volume (IID)

(d) Traffic Volume (Non-IID)

FIGURE 5. Comparison of convergence rate under IID [(a), (c)] and Non-IID [(b), (d)] data distributions for two learning tasks with convex [(c), (d)] and non-convex [(a), (b)] loss functions for the traffic prediction and the image classification respectively.

and ii) total cost which is calculated based on compute and bandwidth resources in both the layers of HFL. A lower training cost is preferred as it reduces the burden on already constrained edge system with O-RAN's tight closed loop timescale.

D. PERFORMANCE EVALUATION

Now, we examine the performance of MHORANFed in light of the defined metrics, the relevant baselines, learning tasks, and data distributions under the described experimental settings.

1) IMPACT OF LOCAL TRAINERS' PARTICIPATION METHOD

Keeping the value of $\rho = 0.5$ (implying a balanced trade-off between learning time and resource usage costs) for MHORANFed, we compared the performance of the baselines in terms of training costs (Fig. 6) and convergence rate (Fig. 5). The key differentiator is their local trainers' selection method. We can also observe the exact number of global rounds required by each method in Table 4. In general MHORANFed outperforms clustering based MACFL and RL based FedPPO among other HFL variants, advocating the importance of our proposed joint optimization based selection.

2) IMPACT OF LOSS FUNCTION TYPE

The convergence in the non-convex case (CIFAR-10) appears to be more sensitive to the non-IID data distribution, as seen by the more pronounced differences in the convergence patterns between the IID and Non-IID CIFAR-10 plots in Fig. 5a and 5b.

In contrast, the RMAE curves for the Traffic dataset show a generally smoother and more rapid decrease, particularly in the IID setting as can be seen in Fig. 5d. MHORANFed effectively handles the non-convex loss function in the CIFAR datasets, achieving high accuracy in both IID and Non-IID settings. However, like other methods, its convergence is somewhat affected by the non-IID distribution, showing a more gradual increase in accuracy. With the convex loss function in the Traffic datasets, Fig. 5c validates that MHORANFed shows a rapid convergence and achieves the lowest RMAE.

3) IMPACT OF DATA HETEROGENEITY

The Non-IID settings significantly impact the convergence behavior and performance of all methods. As illustrated in Fig. 5, the results across the CIFAR and Traffic datasets reveal a consistent trend: data heterogeneity, as represented by the non-IID settings, significantly impacts the

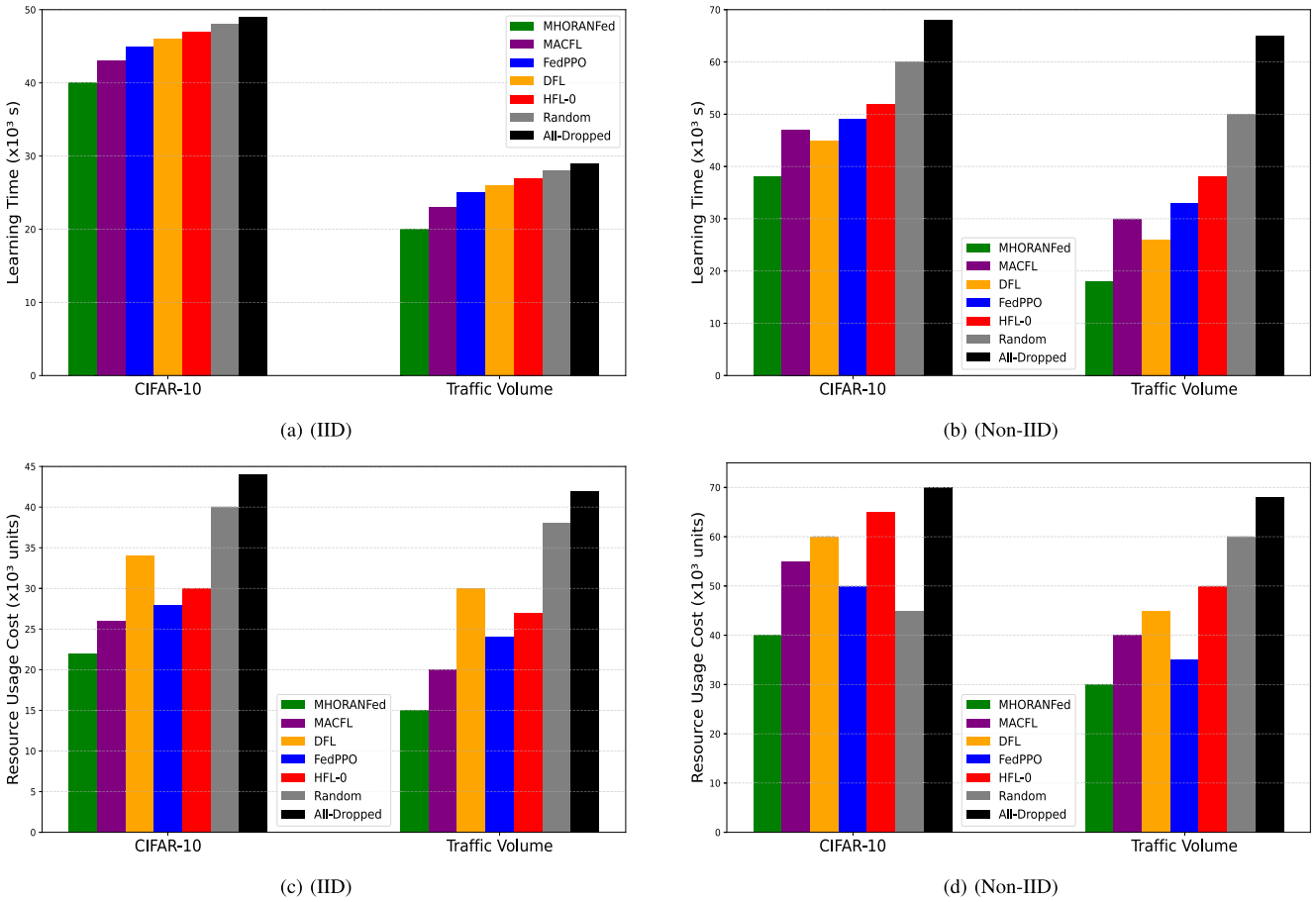

FIGURE 6. Comparison of Training Costs in terms of total Learning Time [(a), (b)] and Resource Usage [(c), (d)] under IID and Non-IID data distributions.

convergence and final performance of all federated learning methods compared to the IID scenarios. In both the CIFAR and Traffic tasks, the convergence curves for all methods are generally slower and sometimes more erratic under non-IID conditions. Furthermore, the final performance metrics (Train Accuracy for CIFAR and RMAE for Traffic) achieved by the methods are typically worse in the non-IID settings than in their IID counterparts. Nonetheless, MHORANFed consistently outperforms other methods across both IID and Non-IID settings and for both CIFAR and Traffic datasets.

On the other hand, Fig. 6 shows that the presence of heterogeneous data distribution leads to higher training costs. While MHORANFed incurs significantly lower learning time and resource usage costs, other baselines show a relatively higher costs with fluctuating performance. This suggests that MHORANFed is more robust and effective in various hierarchical federated learning scenarios.

4) IMPACT OF KEY HYPERPARAMETERS SETTING (SENSITIVITY)

Fig. 7 shows a comparative behaviour of MHORANFed on how well it performs with respect to the centralized training benchmark and multiple combinations of ρ and η. We can see that varying the Pareto trade-off (ρ) affects convergence and higher values don't always guarantee the best outcome. On the other hand, lower values of ρ (e.g., 0.01) can lead to slower convergence. Another key observation is that the performance gap between MHORANFed and the centralized benchmark is often wider in Non-IID scenarios. We can infer through Fig. 7a, 7c, 7b, and 7d that the best performance corresponds to $\rho = 0.5$ and $\eta = 0.01$.

5) IMPACT OF THE NUMBER OF UEs and BSs (SCALABILITY)

We applied two scenarios corresponding to small (2 BSs and 20 UEs) and medium (5 BSs and 100 UEs) scale connections to bring out the impact of scalability. The result is shown in Fig. 8. While the methods converge in both the cases, they are affected by the presence of heterogeneity (non-IID). Nonetheless, MHORANFed requires less number of global rounds to attain the threshold model performance for both the learning tasks.

E. ANALYSIS

The superior performance of MHORANFed is due to its optimal selection of participating UEs in each global FL

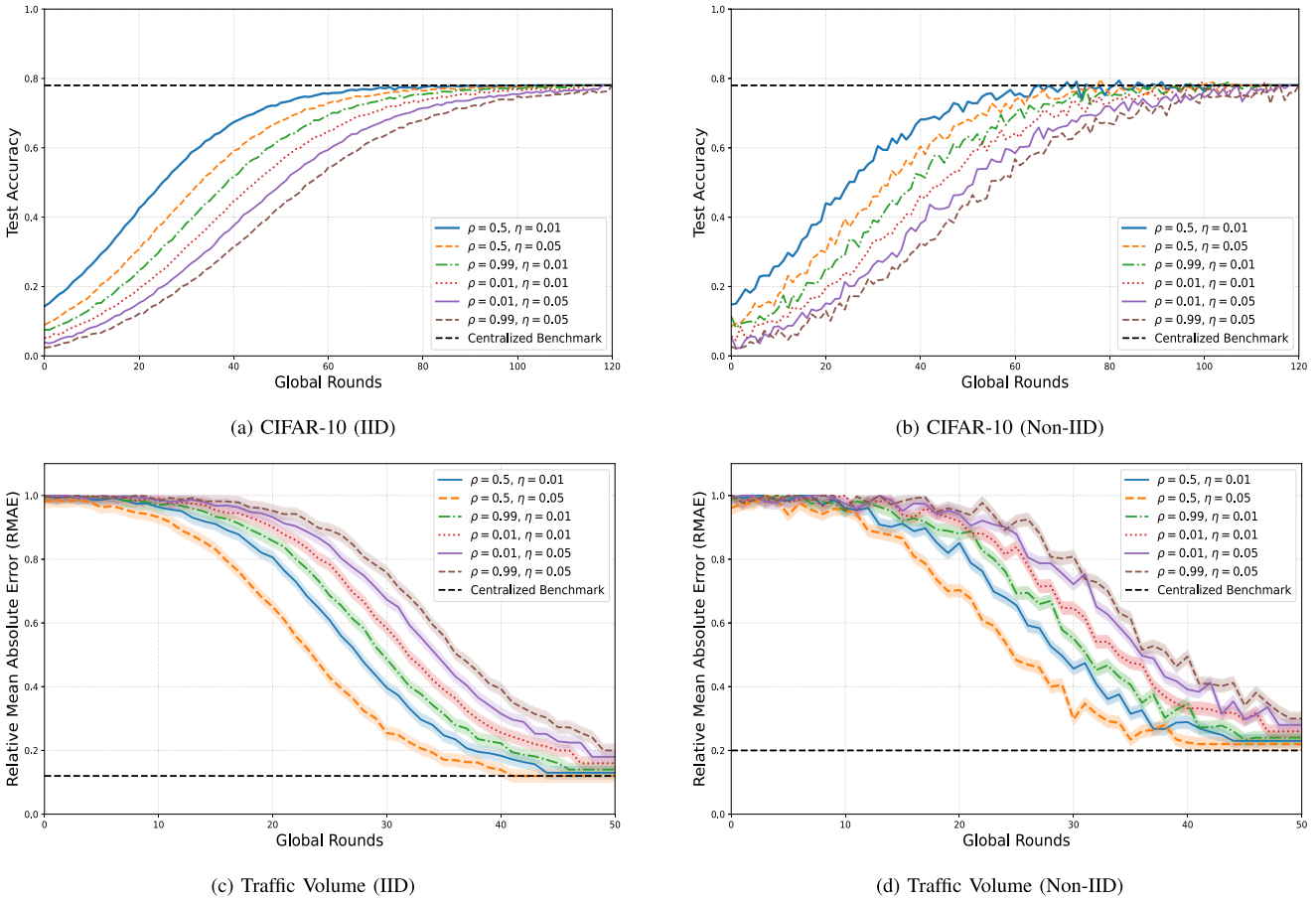

(a) CIFAR-10 (IID)

(b) CIFAR-10 (Non-IID)

(c) Traffic Volume (IID)

(d) Traffic Volume (Non-IID)

FIGURE 7. Performance of MHORANFed under different data distributions, learning tasks, and system hyper-parameters. (a) and (b) are with a Non-Convex Loss Function, while (c) and (d) are with a Convex Loss Function.

round and the corresponding bandwidth resource allocation to only the contributing UEs in the ongoing model training. MHORANFed converges faster because it is biased towards those temporally associated set of local trainers that require less processing time. So, the UEs with higher compute tends to be favoured over increasing global rounds. On the other hand, the other baselines do not employ any such technique. *DFL* while reduces the training time in each global round by fixing a deadline for the local trainers, it also requires more number of global rounds to converge. This results in overall a higher learning time. In terms of the resource cost, MHORANFed critically assigns the bandwidth for the communication channel between a BS and its associated UEs for uploading the updated model parameters. Therefore, it minimizes the total resource usage cost. By outperforming clustering-based MACFL and RL-based FedPPO, MHORANFed's HO delay aware optimization based selection of local trainers proves to be more effective, highlighting the importance of this proposed approach. Despite the increased training costs associated with heterogeneous data for all methods, MHORANFed incurs significantly lower learning time and resource usage costs compared to the baselines. MHORANFed effectively handles both non-convex (CIFAR) and convex (Traffic) loss functions, achieving high accuracy and rapid convergence, respectively. While its convergence is somewhat affected by non-IID distribution in the non-convex case, it still maintains superior performance. MHORANFed requires fewer global rounds to reach the performance threshold in both small and medium-scale network settings, indicating better scalability compared to other methods, especially in the presence of data heterogeneity. MHORANFed consistently achieves better final performance metrics (Train Accuracy for CIFAR and RMAE for Traffic) compared to other methods across both IID and Non-IID data distributions and for both the CIFAR and Traffic datasets. Based on the evaluation outcome, we can infer that MHORANFed demonstrates superior performance and robustness in hierarchical federated learning scenarios, particularly under challenging conditions such as data heterogeneity. These results can be extrapolated to infer the generalization ability of our proposed method as it solves the optimization problem (21) in every global round to get an approximated near-optimal solution. So, it should work for real world use cases where the models are required to be executed with UEs' dynamically changing data. Moreover, since the model is trained on such large datasets, it also has the potential to be scaled over a large

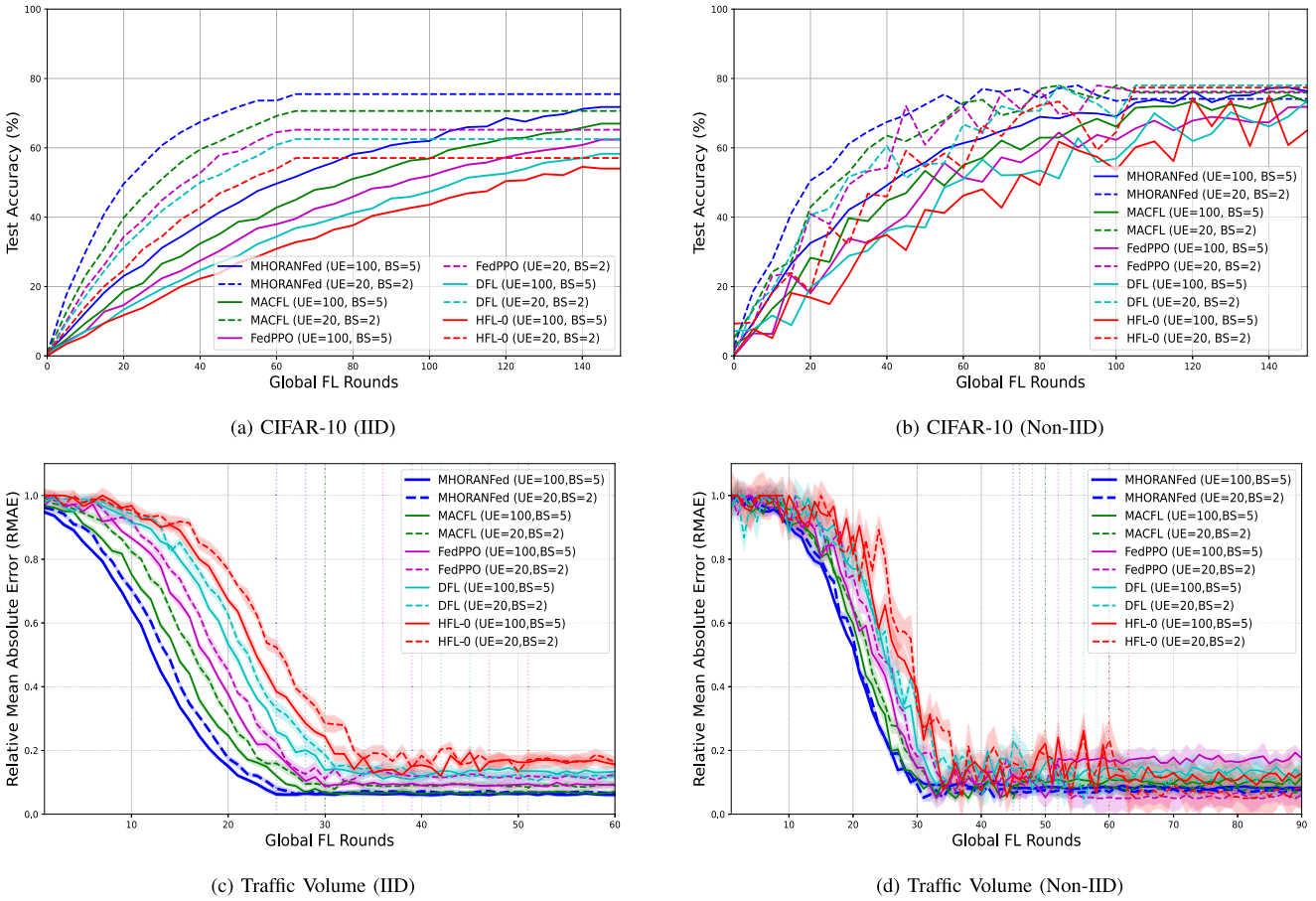

(a) CIFAR-10 (IID)

(b) CIFAR-10 (Non-IID)

(c) Traffic Volume (IID)

(d) Traffic Volume (Non-IID)

FIGURE 8. Comparison of scalability with two settings: (i) small scale (2 BSs and 20 UEs), (ii) medium scale (100 UEs and 5 BSs) under IID and Non-IID data distributions, convex and non-convex loss functions for the image classification and traffic prediction learning tasks respectively.

number of UEs with smaller dataset sizes. Applications such as fulfilling the QoS of connected cars, the key network traffic indicators can be used to predict the required radio resource using MHORANFed exploiting its fast and reliable convergence property.

VI. CONCLUSION

In this paper, we have introduced MHORANFed, a novel optimization algorithm tailored for HFL within the O-RAN architecture. By addressing the dynamic nature of mobile networks, particularly UE handovers, our proposed MHORANFed algorithm minimizes FL model training time and resource usage costs while maintaining high model accuracy. By addressing mobility-related challenges in FL for O-RAN, this research not only enhances the practicality and efficiency of HFL models but also lays the foundation for enabling a broad range of next-generation use cases. This work bridges a critical gap, pushing the boundaries of what intelligent, privacy-preserving, and resource-efficient networks can achieve in highly dynamic environments. These improvements are critical for enabling advanced 5G applications, such as autonomous driving and augmented reality, which demand both high performance and stringent privacy standards. By effectively managing the challenges posed by UE handovers and the dynamic sets of associated devices, MHORANFed paves the way for more flexible, intelligent, and efficient 5G network optimization. Future research will delve into further refining our algorithm and exploring its application in other evolving network paradigms, ensuring that the potential of FL in enhancing O-RAN architectures is fully realized.

ACKNOWLEDGMENT

The authors thank NSERC, VMware Canada, and Mitacs for supporting this research through under Grant ALLRP 577577-22.

REFERENCES

[1] H. N. Qureshi, M. Manalastas, S. M. A. Zaidi, A. Imran, and M. O. Al Kalaa, "Service level agreements for 5G and beyond: Overview, challenges and enablers of 5G-healthcare systems," *IEEE Access*, vol. 9, pp. 1044–1061, 2021.

[2] S. Marinova and A. Leon-Garcia, "Intelligent O-RAN beyond 5G: Architecture, use cases, challenges, and opportunities," *IEEE Access*, vol. 12, pp. 27088–27114, 2024.

[3] M. Polese, L. Bonati, S. D'Oro, S. Basagni, and T. Melodia, "Understanding O-RAN: Architecture, interfaces, algorithms, security, and research challenges," *IEEE Commun. Surveys Tuts.*, vol. 25, no. 2, pp. 1376–1411, 2nd Quart., 2023.
[4] "O-RAN empowering vertical industry: Scenarios, solutions and best practice," O-RAN Alliance, Alfter, Germany, Tech. Rep., 2023.
[5] A. Lacava et al., "Programmable and customized intelligence for traffic steering in 5G networks using open RAN architectures," *IEEE Trans. Mobile Comput.*, vol. 23, no. 4, pp. 2882–2897, Apr. 2023.
[6] B. McMahan, E. Moore, D. Ramage, S. Hampson, and B. A. Y. Arcas, "Communication-efficient learning of deep networks from decentralized data," in *Proc. Artif. Intell. Statist.*, 2017, pp. 1273–1282.
[7] H. Zhou, Y. Zheng, H. Huang, J. Shu, and X. Jia, "Toward robust hierarchical federated learning in Internet of Vehicles," *IEEE Trans. Intell. Transp. Syst.*, vol. 24, no. 5, pp. 5600–5614, May 2023.
[8] Z. Xu et al., "HierFedML: Aggregator placement and UE assignment for hierarchical federated learning in mobile edge computing," *IEEE Trans. Parallel Distrib. Syst.*, vol. 34, no. 1, pp. 328–345, Jan. 2023.
[9] S. Luo, X. Chen, Q. Wu, Z. Zhou, and S. Yu, "HFEL: Joint edge association and resource allocation for cost-efficient hierarchical federated edge learning," *IEEE Trans. Wireless Commun.*, vol. 19, no. 10, pp. 6535–6548, Oct. 2020.
[10] A. K. Singh and K. K. Nguyen, "Communication efficient compressed and accelerated federated learning in open RAN intelligent controllers," *IEEE/ACM Trans. Netw.*, vol. 32, no. 4, pp. 1–15, Aug. 2024.
[11] A. K. Singh and K. K. Nguyen, "Joint selection of local trainers and resource allocation for federated learning in open RAN intelligent controllers," in *Proc. IEEE Wireless Commun. Netw. Conf. (WCNC)*, Apr. 2022, pp. 1874–1879.
[12] Y. Gao, Y. Zhao, and H. Yu, "Multi-tier client selection for mobile federated learning networks," in *Proc. IEEE Int. Conf. Multimedia Expo (ICME)*, Jul. 2023, pp. 666–671.
[13] B. H. Prananto, Iskandar, and A. Kurniawan, "A new method to improve frequent-handover problem in high-mobility communications using RIC and machine learning," *IEEE Access*, vol. 11, pp. 72281–72294, 2023.
[14] M. Noor-A-Rahim, Z. Liu, H. Lee, G. G. M. N. Ali, D. Pesch, and P. Xiao, "A survey on resource allocation in vehicular networks," *IEEE Trans. Intell. Transp. Syst.*, vol. 23, no. 2, pp. 701–721, Feb. 2022.
[15] R. Karmakar, G. Kaddoum, and S. Chattopadhyay, "Mobility management in 5G and beyond: A novel smart handover with adaptive time-to-trigger and hysteresis margin," *IEEE Trans. Mobile Comput.*, vol. 22, no. 10, pp. 5995–6010, Oct. 2023.
[16] F. P.-C. Lin, S. Hosseinalipour, N. Michelusi, and C. G. Brinton, "Delay-aware hierarchical federated learning," *IEEE Trans. Cognit. Commun. Netw.*, vol. 10, no. 2, pp. 674–688, Apr. 2024.
[17] Y. Xu, B. Qian, K. Yu, T. Ma, L. Zhao, and H. Zhou, "Federated learning over fully-decoupled RAN architecture for two-tier computing acceleration," *IEEE J. Sel. Areas Commun.*, vol. 41, no. 3, pp. 789–801, Mar. 2023.
[18] S. Liu, G. Yu, X. Chen, and M. Bennis, "Joint user association and resource allocation for wireless hierarchical federated learning with IID and non-IID data," *IEEE Trans. Wireless Commun.*, vol. 21, no. 10, pp. 7852–7866, Oct. 2022.
[19] C. Feng, H. H. Yang, D. Hu, Z. Zhao, T. Q. S. Quek, and G. Min, "Mobility-aware cluster federated learning in hierarchical wireless networks," *IEEE Trans. Wireless Commun.*, vol. 21, no. 10, pp. 8441–8458, Oct. 2022.
[20] J. Liu et al., "Adaptive asynchronous federated learning in resource-constrained edge computing," *IEEE Trans. Mobile Comput.*, vol. 22, no. 2, pp. 674–690, Feb. 2023.
[21] C. T. Dinh et al., "Federated learning over wireless networks: Convergence analysis and resource allocation," *IEEE/ACM Trans. Netw.*, vol. 29, no. 1, pp. 398–409, Feb. 2021.
[22] Y. Cao, S.-Y. Lien, Y.-C. Liang, K.-C. Chen, and X. Shen, "User access control in open radio access networks: A federated deep reinforcement learning approach," *IEEE Trans. Wireless Commun.*, vol. 21, no. 6, pp. 3721–3736, Jun. 2022.
[23] Y. Cao, S.-Y. Lien, Y.-C. Liang, and K.-C. Chen, "Federated deep reinforcement learning for user access control in open radio access networks," in *Proc. IEEE Int. Conf. Commun. (ICC)*, Jul. 2021, pp. 1–6.
[24] Z. Zhao, A. Li, R. Li, L. Yang, and X. Xu, "FedPPO: Reinforcement learning-based client selection for federated learning with heterogeneous data," *IEEE Trans. Cognit. Commun. Netw.*, early access, Mar. 4, 2025, doi: 10.1109/TCCN.2025.3547751.
[25] *Technical Specification: 5G NG-RAN Architecture Deacription*, ETSI 3GPP, Sophia Antipolis, France, Sep. 2024.
[26] J. Kim et al., "A formally verified security scheme for Inter-gNB-DU handover in 5G vehicle-to-everything," *IEEE Access*, vol. 9, pp. 119100–119117, 2021.
[27] A. R. Prasad, S. Arumugam, B. Sheeba, and A. Zugenmaier, "3GPP 5G security," *J. ICT Standardization*, vol. 6, no. 1, pp. 137–158, Jan. 2018.
[28] L. Vandenberghe and S. Boyd, "Semidefinite programming," *SIAM Rev.*, vol. 38, no. 1, pp. 49–95, Mar. 1996, doi: 10.1137/1038003.
[29] S. Diamond and S. Boyd, "CVXPY: A Python-embedded modeling language for convex optimization," *J. Mach. Learn. Res.*, vol. 17, no. 83, pp. 1–5, Jan. 2016.
[30] H. Lee, Q. Song, and J. Honorio, "Support recovery in sparse PCA with incomplete data," in *Proc. Adv. Neural Inf. Process. Syst.*, A. H. Oh, A. Agarwal, D. Belgrave, and K. Cho, Eds., 2022, pp. 1–18. [Online]. Available: https://openreview.net/forum?id=x5ysKCMXR5s
[31] C. Ma et al., "Distributed optimization with arbitrary local solvers," *Optim. Methods Softw.*, vol. 32, no. 4, pp. 813–848, Jul. 2017.
[32] S. Wang et al., "Adaptive federated learning in resource constrained edge computing systems," *IEEE J. Sel. Areas Commun.*, vol. 37, no. 6, pp. 1205–1221, Jun. 2019.
[33] A. Krizhevsky, V. Nair, and G. Hinton. *CIFAR-10 (canadian Institute for Advanced Research)*. Accessed: Apr. 4, 2025. [Online]. Available: http://www.cs.toronto.edu/
[34] L. Deng, "The MNIST database of handwritten digit images for machine learning research [best of the web]," *IEEE Signal Process. Mag.*, vol. 29, no. 6, pp. 141–142, Nov. 2012.
[35] J. S. Rojas. (2020). *IP Network Traffic Flows Labeled With 87 Apps*. Accessed: Apr. 2, 2025. [Online]. Available: https://wwwkaggle.com/datasets/jsrojas/ip-network-traffic-flows-labeled-with-87-apps

AMARDIP KUMAR SINGH (Student Member, IEEE) received the B.Sc. and M.Sc. degrees from Presidency University (formerly Presidency College under the University of Calcutta), India, and the M.Tech. degree in computer science and technology from Jawaharlal Nehru University, India, where he examined machine learning algorithms for heart disease classification. He is currently pursuing the Ph.D. degree with the Department of Electrical Engineering, École de Technologie Supérieure (ÉTS), Montreal, Canada. His Ph.D. research explores the design and optimization of federated learning frameworks for next-generation mobile networks enabled by open radio access networks (Open RAN). His academic foundation is rooted in mathematics. He is also a former MITACS Fellow.

KIM KHOA NGUYEN is currently a Professor with the Department of Electrical Engineering and the Founder and the Director of the IoT and Cloud Computing Laboratory, École de Technologie Supérieure, University of Quebec, Montreal, Canada. He holds the VMware-Broadcom Industrial Chair in Multi-Cloud Service Grid and Edge AI. He led research and development in several large-scale projects with world-class corporations, such as VMware, Ericsson, Ciena, Telus, InterDigital, and Ultra Electronics. He is the author of more than 200 publications and holds several industrial patents. His research interests include network optimization, wireless communications, optical networks, cloud computing, the IoT, 5G, machine learning, AI, and green ICT. He was a recipient of the Microsoft's Azure Global IoT Contest Award in 2017, the Ciena's Aspirational Prize in 2018, and the IEEE Future Internet's "Connecting the Unconnected" Award in 2023.